

Article

MEMS Vibrational Power Generator for Bridge Slab and Pier Health Monitoring

Katsufumi Hashimoto ^{1,*}, Tomoki Shiotani ¹, Hiroyuki Mitsuya ² and Kai-Chun Chang ¹ 

¹ Department of Civil and Earth Resources Engineering, Graduate School of Engineering, Kyoto University, Kyoto 615-8540, Japan; shiotani.tomoki.2v@kyoto-u.ac.jp (T.S.); chang.kaichun.4z@kyoto-u.ac.jp (K.-C.C.)

² R&D Center, Saginomiya Seisakusho, Inc., Saitama 350-1395, Japan; hiro-mitsuya@saginomiya.co.jp

* Correspondence: hashimoto.katsufumi.8a@kyoto-u.ac.jp; Tel.: +81-75-383-3496

Received: 29 October 2020; Accepted: 18 November 2020; Published: 21 November 2020



Abstract: Micro energy harvesters (MEH) based on microelectromechanical systems (MEMS) are rapidly developing, providing a green and virtually infinite energy source. The electrostatic vibratory power generator outputs electric power when it vibrates, motivating us to apply it to vibrating civil infrastructures excited by ambient and daily traffic loadings. In this study, an innovative monitoring system utilizing MEH devices was proposed for detecting slab damage and pier scours for bridge structures. Its performance was numerically investigated with finite element models, where the damage in slabs was modeled with a reduced Young's modulus and scours with fixed boundaries of inclined depth. It was shown that the powers generated at each MEH varied as the target structure's modal frequency shifted and amplitude changed by damage or scour. A power generation index was proposed to identify slab damage and a reference-free method was introduced to detect uneven pier scours. Utilizing an electrostatic vibration-based MEH (MEMS vibrational power generator), this pioneering study showed that MEMS vibrational power generators can work as sensors for an infrastructure structural health monitoring system.

Keywords: MEMS; Micro Energy Harvester; structural health monitoring; vibration; frequency; amplitude; pier; scouring

1. Introduction

1.1. Management of Aging Structures

Many infrastructures in Japan were built in the mid-1900s when there was high economic growth and more than a quarter of all the bridges in Japan, at present, are more than 50 years old. This number will reach up to approximately 50% in the next ten years. Timely inspection, monitoring, and appropriate maintenance for safety purposes are eagerly required. In addition, it is necessary to manage the financial labor resources for effective and efficient structural health monitoring of those aging infrastructures. Approximately 70% of the bridges in Japan are short- to median-span bridges managed by local governments, and the ratio of those bridges (>2 m length, which is defined in Japanese inspection protocols of the Ministry of Land, Infrastructure, Transport and Tourism) over 50 years old will reach to 67% in the next 20 years [1]. A real-time monitoring system that can detect potential damage or deterioration is necessary to tackle the globally challenging issues of disaster mitigation and social safety.

1.2. Deterioration of Bridge Structure Components

Superstructure, which consists of beams and slabs, etc., is the span that directly supports live loads. On the other hand, substructure, which consists of piers and abutments, etc., supports the

entire bridge structure and loads on the underground footings. Their long-term deterioration due to external loadings in the service environment is vastly reported as regards fatigue damage with crack propagation in concrete slabs and pier scours due to heavy rains and floods [2,3]. Damage in slabs is mostly found in highway (motorway) superstructures, while pier scouring is naturally recognized as the main cause of damage and failure of bridges over waterways.

In steel–concrete composite decks, the often-occurring damage type is fatigue damage due to numerous repeating traffic overloads [4,5]. The final form of this damage is well known as large horizontal cracks in steel–concrete composite slabs [5]. As it is difficult to visually (by visual inspections) detect internal damage, which potentially affects structural performance [6], it becomes a very serious problem for highway reinforced concrete (RC) structures [7].

Scouring is one of various problems that occur in the structural performance deterioration of bridges. It is a phenomenon due to insufficient rooting at the foundation of the pier due to disappearance of riverbed sediment with running water, which results in a loss of bridge stability [8]. It was pointed out that relatively few vibration-based damage detection studies focused on substructures (especially piers and foundations), as opposed to the studies on superstructures or entire bridges [9]. Since it has been particularly confirmed that vibration mode shapes of bridge piers are relatively simple, it is possible to detect pier scouring by the change in modal amplitude ratio in impact vibration tests [10,11]. However, it is still too early to conclude that it is the optimal test method because it is risky to impact tall piers from the cap and it is almost impossible to constantly perform the test [12].

Appropriate inspection, monitoring, and maintenance of aging structures are required for safety purposes. However, in the above-mentioned conventional measurement methods, the cable connections to the power grid may cause a mechanical limitation of inspection and inefficient in situ monitoring operation. A real-time monitoring system that can detect the damage and deterioration of target structures is of great help in globally challenging disaster mitigation and social safety issues. In order to achieve a safe civil infrastructure network, a compact, easy-to-use, small-sized, and self-sustaining device with a stand-alone power system is ideal to be applied for entire bridge structural health monitoring.

1.3. Development of Sensors with MEMS Technologies

It is expected that various sensing devices would be installed in infrastructure and a lot of services utilizing big data would be created and socially provided by the Internet [13–15]. In a “Trillion sensors society”, which is aimed for by the TSensors (Trillion Sensors) project [16,17], it is clearly indicated that our society and life are greatly changed in all fields, such as medical health care, agriculture, environment, and infrastructure, and the whole society is connected to the network by many sensor terminals.

In infrastructure monitoring, developments in sensor device and IoT technology are indispensable. At the same time, it is considered that a self-powered (battery-free) device is necessary to build the sensor network and deliver reliable and long-term performance for civil infrastructures in their service life with environmental conditions. Energy harvesters are categorized into three types depending on the operational principles: electromagnetic transduction [18,19], electrostatic transduction [18,20], and piezoelectric transduction [18,21]. Several studies have been conducted on characterizing the environment- and bridge structural type-dependent vibrations and on quantifying the powers harvested from those vibrations using comb-shaped silicon electrets (see Figure 1) [22].

In the electret electrostatic microelectromechanical systems (MEMS) energy harvester, as shown in Figure 2, the electret is a vibrating mass supported by a spring and forms a variable capacitance when it is facing a fixed electrode through an air gap. It is possible to output the current with power generation based on the frequency response synchronized with the movement of the electrode (oscillation). The structure can be designed to efficiently obtain the generation amount only in a certain frequency band [22]. As a small wireless device of coin size for the purpose of frequency detection of environmental vibration, it can be easily mounted without any space and wiring problems.

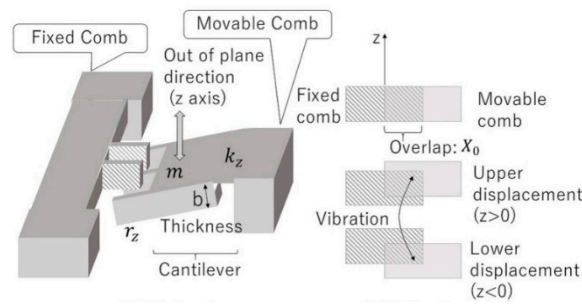


Figure 1. A schematic model of the vibration energy harvester [22].

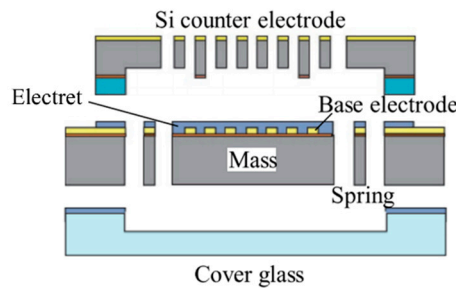


Figure 2. Cross-sectional view of microelectromechanical systems (MEMS) vibration energy harvester.

A vibration-based micro energy harvester (MEH) device is proposed to monitor the health of RC concrete slabs and pier scours in this study. MEH devices are introduced with microelectromechanical systems (MEMS) technology. They harvest micro energy from its environmental energy source such as light, wind, heat, and electromagnetic field vibration and convert it into electric energy. If they can be integrated into (or embedded in) infrastructure monitoring sensors, they can supply the sensors' power and, to a certain extent, make the sensors self-sustaining, needing no cable connection to the electricity power grid.

In terms of power-generating capacity, light-, vibration-, and wind-sourced MEH devices perform comparatively better than the other choices, such as heat- and electromagnetic-sourced MEH. Among the three types of MEH (light-, vibration-, and wind-based), a vibration-based MEH device is the only one that can function in lightless, windless, dark, or night conditions and inside the box girders. Therefore, a vibration-based MEH is proposed for bridge structural health monitoring. The vibration-based MEH device used herein (see Figure 3) was identical to those proposed in previous studies [22], which is an inexpensive coin-sized device that can generate over 100 μW RMS (root mean square) of output electric power under 0.03 G_{RMS} accelerations.

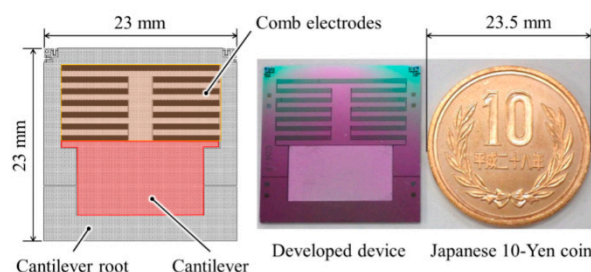


Figure 3. A photograph of the applied vibration-based micro energy harvester (MEH) device (Device size is 23 × 23 mm) [22].

1.4. MEMS Vibrational Power Generator

As described above, the vibration power generation device (MEMS vibrational power generator) has a fixed and a movable comb electrode. Presuming that the same impedance as the internal

impedance of the vibration power generator is connected to the device, the expected RMS output power can be calculated from Equations (1) and (2), where the conversion efficiency from the linear equivalent circuit of the electrostatic actuator is considered [22].

$$P = \frac{ma^2Q}{4\omega_0} \cdot \eta \quad (1)$$

$$\eta = \frac{1}{1 + \left(\frac{kC_0}{QA^2}\right)^2} \quad (2)$$

where P is power generation amount [W], m is mass [kg], a is acceleration [m/s^2], Q is quality factor [-], ω_0 is angular frequency [rad/s], η is efficiency [-], k is spring constant [N/m], C_0 [F] is electrostatic capacity, and A is force coefficient [C/m].

The effective value is the root mean square (RMS) of all instantaneous values within a certain interval, which means the power contained in the vibration waveform. Since all values other than the acceleration are determined by the structure of the MEMS vibrational power generator, the power generation depends only on the magnitude of the effective acceleration value. Knowing that acceleration is proportional to vibration amplitude and frequency squared, it is expected that the generated energy would increase as amplitude and frequency increase.

The force factor A is expressed by Equation (3) and the relationship between the force factor and the current I (short circuit current) is expressed by Equation (4).

$$A = \frac{2n\epsilon_0 bE}{d} \quad (3)$$

$$I = Av \quad (4)$$

where n is number of comb electrodes, ϵ_0 is the permittivity of the vacuum [F/m], b is the thickness of the comb electrode [m], E is the charged voltage [V], d is the gap between the fixed and the movable comb electrodes [m], and v is the vibration speed [m/s_{RMS}].

Table 1 shows the design parameters of the MEMS vibrational power generator which is investigated in this study.

Table 1. Structural and material properties of MEMS vibrational power generator.

| | |
|--|------------------------|
| n : number of comb electrode | 500 |
| ϵ_0 [F/m]: permittivity of vacuum | 2.13×10^{-15} |
| b [m]: thickness of comb electrode | 3.00×10^{-4} |
| E [V]: charged voltage | 400 |
| d [m]: gap between the fixed and the movable comb electrodes | 1.60×10^{-4} |

1.5. Objective

This study focuses on bridge structural health monitoring by installing on slabs and piers the vibration-based power generation devices, which can generate power by converting environmental vibrations into electric energy by electrostatic induction and can detect slab damage and pier scours by the change in the generated energy. An energy generation index to detect slab damage and a reference-free method to detect uneven pier scour are proposed. To illustrate and verify them, numerical slab models and pier models are constructed, and their modal frequencies and mode shapes are obtained by eigenvalue analyses. Damage-induced change in modal frequency and mode shapes are investigated, in which the analytical details are given in Section 2. The energy generated from the vibrations of the numerical models are calculated and the proposed methods are introduced, with their verification in Section 3. Finally, several concluding remarks are provided in the last section.

2. Finite Element Analysis for Bridge Structures with Damage and Deterioration

2.1. Outline of Eigen-Modal Analysis

It is known that the dominant vibration frequency of a structure generally decreases when the stiffness of bridge components is reduced with a sort of material and structural deterioration. In this study, a vibration analysis was conducted on slab and pier models with several damage scenarios to reveal the frequency change and modal amplitude change caused by damage. For the slab model, it consisted of six uniform panels, whose material properties were tuned down to model damage. For the pier model, it consisted of four identical panels and the riverbed level was tuned down to model scouring.

This numerical vibration analysis was conducted using finite element analysis software suite ABAQUS 6.14. After the finite element models' construction, eigenvalue analysis was conducted to obtain the modal properties for each model. Based on the vibration analysis results, generated power is calculated according to the MEH device structure. The eigenvalue problem for a finite element model is involved in solving the eigenequation shown in Equation (5).

$$Kx = \lambda Mx \tag{5}$$

where K is the global stiffness matrix (sparse positive definite matrix of size $n \times n$), M is the global mass matrix (sparse positive-definite matrix of size $n \times n$), λ is the eigenvalue, x is the eigenvector, and n is the number of degrees of freedom. In ABAQUS, the Lanczos inverse power method is used to solve the eigenvalue problem, especially in a case where lower vibration modes are of more concern.

2.2. Slab Model with Concrete Material Deterioration

Figure 4 shows the slab model in this study, which consists of six concrete panels and two steel footing girders of I shape. Simplifying the model, there is no reinforcement simulated in geometrical information. They were all modelled with solid elements, in which the panels as well as the panels and girders are rigidly connected. To investigate the damage (deterioration)-induced modal property change, four cases in Figure 5 were considered and this study only investigated single panel damage: one intact case (labelled as Case 0) and three damage cases (Case 1, 2, and 3). Case 0 served as the reference, whose material properties for concrete and steel bars were set as those given by the design drawings, while Cases 1, 2, and 3 had their first (P1), second (P2), and third panel (P3) damaged, respectively, whose concrete material properties were tuned down (see Table 2). Steel bars were considered intact all the time. As mentioned previously, eigenvalue analysis was conducted for the four cases to obtain their modal frequencies and modal shapes.

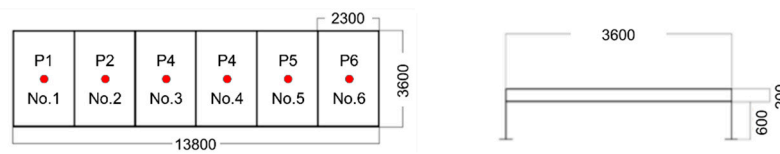
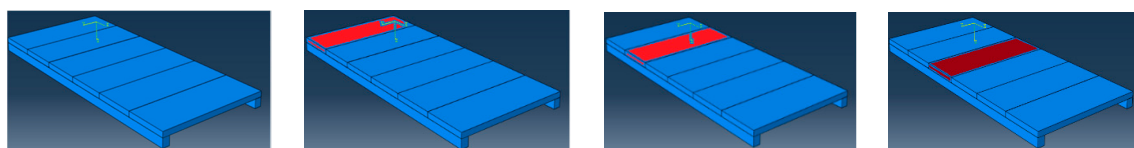


Figure 4. Slab model geometry (Unit: mm).



(a) Case 0: Intact (b) Case 1: P1 deteriorated (c) Case 2: P2 deteriorated (d) Case 3: P3 deteriorated

Figure 5. FEM (Finite Element Method) models for a slab with simulated damage.

Table 2. Material properties in FEM for the slab model.

| Materials | Young’s Modulus [GPa] | Poisson’s Ratio | Density [kg/m ³] |
|-------------------------------|-----------------------|-----------------|------------------------------|
| Intact concrete (Panel) | 30 | 0.2 | 2450 |
| Steel (I shape girder) | 210 | 0.3 | 7850 |
| Deteriorated concrete (Panel) | 7.5 | 0.2 | 2450 |

2.3. Pier Model with Scour

The pier’s dimensions and the FE model are shown in Figure 6. The observation points are marked by red points No. 1, 2, and 3, where the powers generated by the MEMS vibrational power generator were to be calculated. The concrete material properties are as follows: elastic modulus 30 GPa, Poisson’s ratio 0.2, and density 2400 kg/m³. The *x*-axis pointed toward the river flow direction (perpendicular to bridge longitudinal), the *y*-axis toward the bridge longitudinal, and the *z* axis toward bridge transverse.

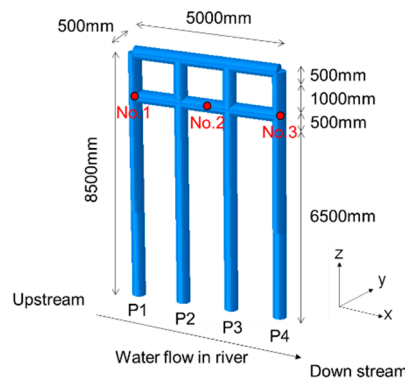


Figure 6. FEM models for the pier.

Two cases were considered: one free from and the other one subject to scouring. As shown in Figure 7, the scouring-free pier model had a uniform riverbed of height 3000 mm and the scouring pier model had an inclined riverbed linearly varying from 500 mm at P1 (upstream side) to 3000 mm at P4 (downstream side). The riverbeds were modelled by fixed boundary conditions for simplicity.

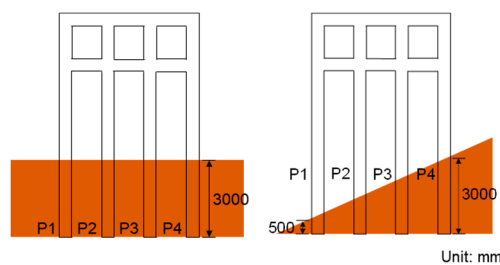


Figure 7. Riverbed geometry with/out simulated scour.

2.4. Eigenvalue Analysis Results

2.4.1. Slab Model

For all slab cases (Case 0, 1, 2, and 3), eigenvalue analysis was conducted to obtain their modal frequencies and mode shapes. Table 3 shows the first two bending modal frequencies (Modes 1 and 3) and the first torsion mode (Mode 2). As expected, the three modal frequencies in Case 1, 2, and 3 were all smaller than those in Case 0; when damage occurred somewhere in the slab (Case 1, 2, and 3), the modal frequency dropped.

Table 3. Vibration frequencies of slab models (Unit: Hz).

| Vibration Mode | Case 0 (Intact) | Case 1 | Case 2 | Case 3 |
|---------------------|-----------------|--------|--------|--------|
| Mode 1: 1st bending | 5.98 | 5.79 | 5.49 | 5.25 |
| Mode 2: 1st torsion | 11.46 | 10.44 | 10.67 | 10.83 |
| Mode 3: 2nd bending | 19.90 | 14.94 | 16.82 | 17.80 |

However, it is difficult to localize the damage in the slab merely from the frequency change. Comparing the three modal frequencies from Case 1, 2, and 3, no clues are found to localize the damage. This is because modal frequencies do not provide any spatial information. To localize damage while focusing on mode shapes (e.g., see Figure 8 for Case 0), it is proposed to install the MEH devices on multiple panels to catch the relative change in energies harvested from different locations. The proposal is further discussed in Section 3.

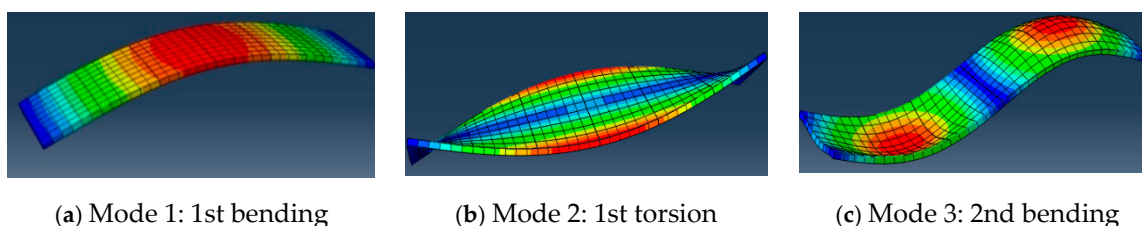


Figure 8. Vibration mode shapes of slab model (Intact: Case 0).

2.4.2. Pier Model

Similarly, for the two cases (scouring-free and scouring pier models), eigenvalue analysis was conducted to obtain their modal frequencies and mode shapes. Knowing that the pier is a cantilever-like structure, the change in its bottom boundary due to scour conditions would similarly change its vibration properties. Therefore, the FEM model is simplified by omitting the superstructure with little loss of generality on the alteration of vibration behavior. Future and further work would be required to adequately model the boundary condition for the top of the pier with regard to mass and stiffness of the bridge deck.

Table 4 gives the modal frequencies of the first three modes. All three modal frequencies in the scouring case were about 30% smaller than those in the scouring-free case; as expected, the modal frequencies dropped as scouring occurred.

Table 4. Modal frequencies of pier models (Unit: Hz).

| Vibration Mode | Scouring Free | Scouring |
|----------------|---------------|----------|
| 1st | 4.59 | 3.05 |
| 2nd | 8.40 | 6.62 |
| 3rd | 9.90 | 7.14 |

Figure 9 shows the first three mode shapes for both the scouring-free and scouring cases, and Figure 10 shows the relative amplitude for the three observation points and the two cases. It is observed that the 1st mode is a longitudinal bending mode, and when scouring occurred, the relative amplitude in y-direction increased at Point No. 1 but decreased at Point No. 3. The 2nd mode is a torsional mode, and when scouring occurred, the relative amplitude in y-direction increased at Point No. 1 and decreased at Point No. 3. The 3rd mode is a lateral bending mode, and when scouring occurred, the relative amplitude changed little. In addition, the above three modes presented small z-direction amplitude as they are all bending modes, so the vibration in the z-direction is hardly useful in scouring detection.

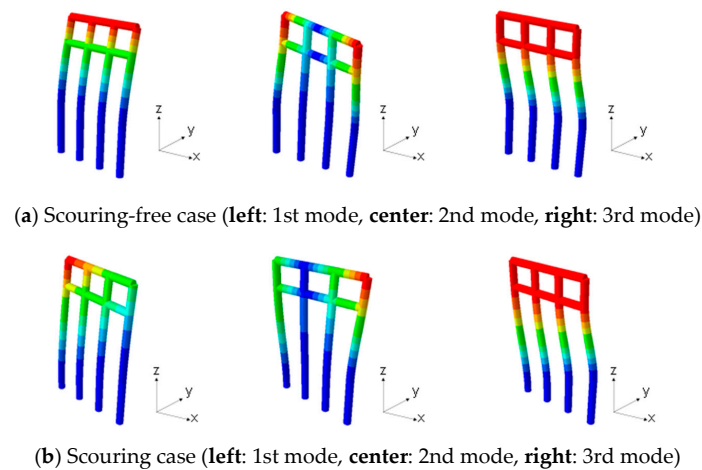


Figure 9. Mode shapes for the pier model.

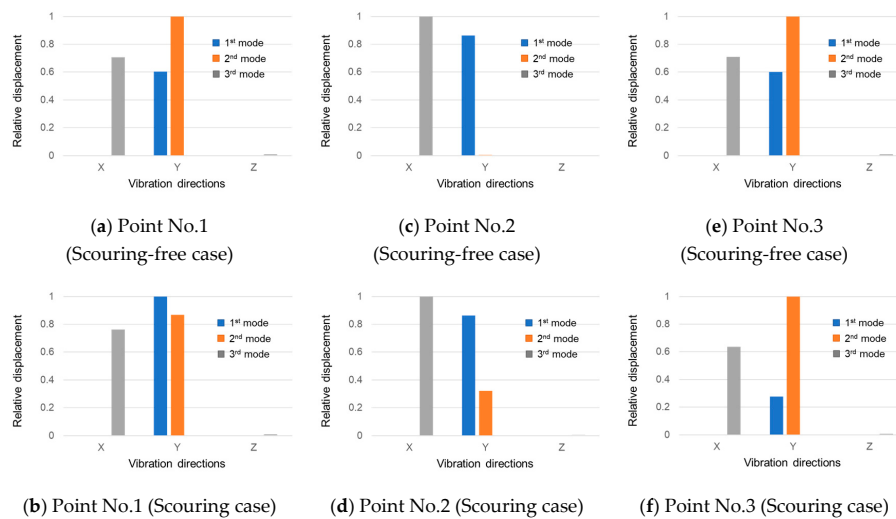


Figure 10. Relative amplitude in mode shapes at observation points for scouring-free and scouring cases.

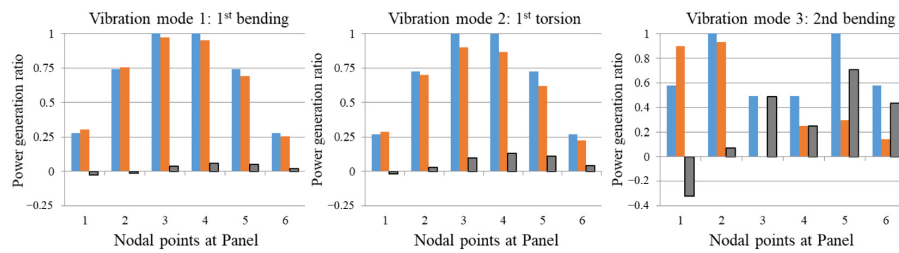
3. Application of MEMS Vibrational Power Generator for Detecting Damage and Deterioration in Bridge Structures

3.1. Numerical Results on Power Generation

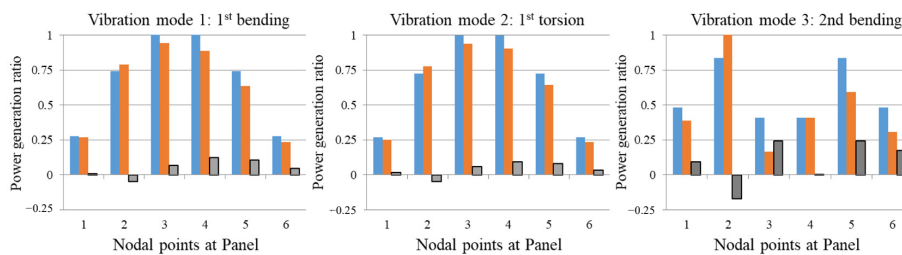
It is assumed in the numerical analysis of this study that the MEH devices are installed on the target slabs at the observation points No. 1 to 6, as shown earlier in Figure 3. Since the proposed MEH devices can be tuned very sensitively to a certain narrow frequency band of interest, it would be reasonable to assume that the devices harvested the energies from slab vibrations of a single mode. From the eigenvalue analysis (Section 2.4), each pier model’s modal frequencies and mode shapes have been provided. For the following numerical analysis, the slabs are assumed to harmonically vibrate with the modal frequency and mode shape of a specified mode, and the harvested powers are calculated using the equations given in Section 1.4 and taking the harmonic vibrations at the observation points of interest as input. The computation on conversion from FEM results to generated energy from the vibrational MEMS device, using Equations (1)–(4), is followed by expressing sinusoidal vibrational waveform as the relationship between displacement and time in accordance to relative vibration amplitude and frequency provided from FEM analysis at each node of interest.

3.2. MEH Power Generation in Slab Models

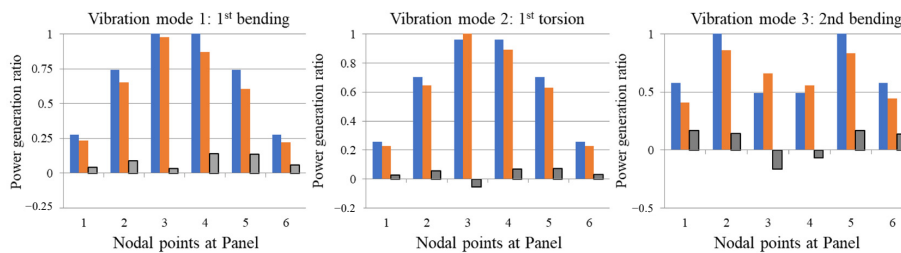
Figure 11 shows the output power generated by the MEH for Cases 0 to 3. In all the subfigures, blue bars represent power generation in Case 0 (intact), where the slab is in a healthy condition, while red bars represent those in deteriorated cases, i.e., Cases 1, 2, or 3. Gray bars show the difference of power generation amount between intact and deteriorated cases. The results indicate that generally, natural frequency decreases when the concrete structure deteriorates, thus the power generation amount also decreases since the main factor for power generation amount is the target structure’s natural frequency. However, at several points, power generation amount increases, even when natural frequency decreases with the damage in RC structure.



(a) Case 1 (Panel 1 damaged) vs. Intact condition



(b) Case 2 (Panel 2 damaged) vs. Intact condition



(c) Case 3 (Panel 3 damaged) vs. Intact condition

■ Case 0 (intact) ■ Case 1, 2, 3 (Panel damaged) ■ Difference

Figure 11. Output power generated by MEH (Slab model).

3.3. Detecting Slab Deterioration Using Vibration-Based MEH

It is observed in Figure 11 that the generated power increases at the deteriorated panels and decreases at the other five panels for nearly all of the cases in three modes of vibration. However, the generated power at the observation points depends on material and structural conditions; hence, it is almost impossible to detect the most deteriorated panel by a direct comparison between the generated powers on different panels. In the case that all panels are intact, their generated powers shall keep in a ratio as presented for Case 0 in Figure 11. Herein, a power generation index I_j ($j = 1$ to 6)

is proposed as follows for the j -th test panel to normalize this location-dependent factor, so as to fairly evaluate the health state of panels at any location.

$$I_j = \frac{\sum_{i=1}^6 \frac{P_i}{P_j}}{6} \text{ for } j = 1, 2, 3, 4, 5, 6 \tag{6}$$

where P_i is the power generated from Panel i in the intact case (Case 0) and P_j the power generated from Panel j in the test case (could be intact or damaged). Generally, all modes could be taken to calculate e_j and to identify damage. Herein, the 3rd mode was selected for its larger power being generated and its outcome is illustrated in Figure 12.

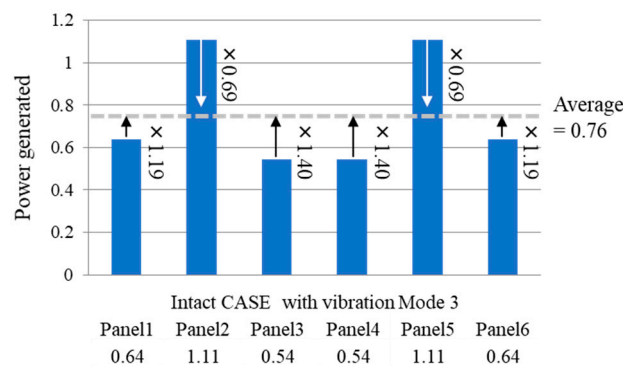


Figure 12. Illustration of Power Index.

Table 5 shows the power generation indices and the modified power generation for Cases 1, 2, and 3, where Panels #1, #2, and #3 are deteriorated, respectively. The results display that all deteriorated panels are pointed out with larger modified power generation, qualifying our proposed index.

Table 5. Application of power generation index for detecting damage with MEH.

| | Panel #1 | Panel #2 | Panel #3 | Panel #4 | Panel #5 | Panel #6 |
|------------------------------|----------|----------|----------|----------|----------|----------|
| Power Generation Index P_i | 1.19 | 0.69 | 1.40 | 1.40 | 0.69 | 1.19 |
| Case1 (generated power) | 0.99 | 1.03 | 0.01 | 0.27 | 0.33 | 0.16 |
| Case 1*PI (modified) | 1.18 | 0.71 | 0.01 | 0.38 | 0.22 | 0.19 |
| Case2 (generated power) | 0.51 | 1.33 | 0.22 | 0.54 | 0.79 | 0.41 |
| Case 2*PI (modified) | 0.61 | 0.92 | 0.31 | 0.76 | 0.54 | 0.48 |
| Case3 (generated power) | 0.45 | 0.95 | 0.73 | 0.61 | 0.92 | 0.49 |
| Case 3*PI (modified) | 0.54 | 0.65 | 1.02 | 0.86 | 0.63 | 0.58 |

3.4. MEH Power Generation in Pier Models

The power generated by the MEH at the observation points No. 1, 2, and 3 (see Figure 6) can be calculated with Equations (1)–(4), as well for both the scouring-free and scouring pier models. Figure 13 shows the generated power for the two models and the first three modes. Note that the power is presented in a relative manner with respect to the maximum power in the same model and the same mode. As expected, the 1st mode generates the most power in the y-direction at all three observation points as it is a longitudinal bending mode; the 2nd mode generates in the y-direction at observation points No. 1 and 3 as it is a torsion mode; the 3rd mode generates in the x-direction at all three observation points as it is a lateral bending mode. Little power is generated in the z-direction (vertical direction) for all modes.

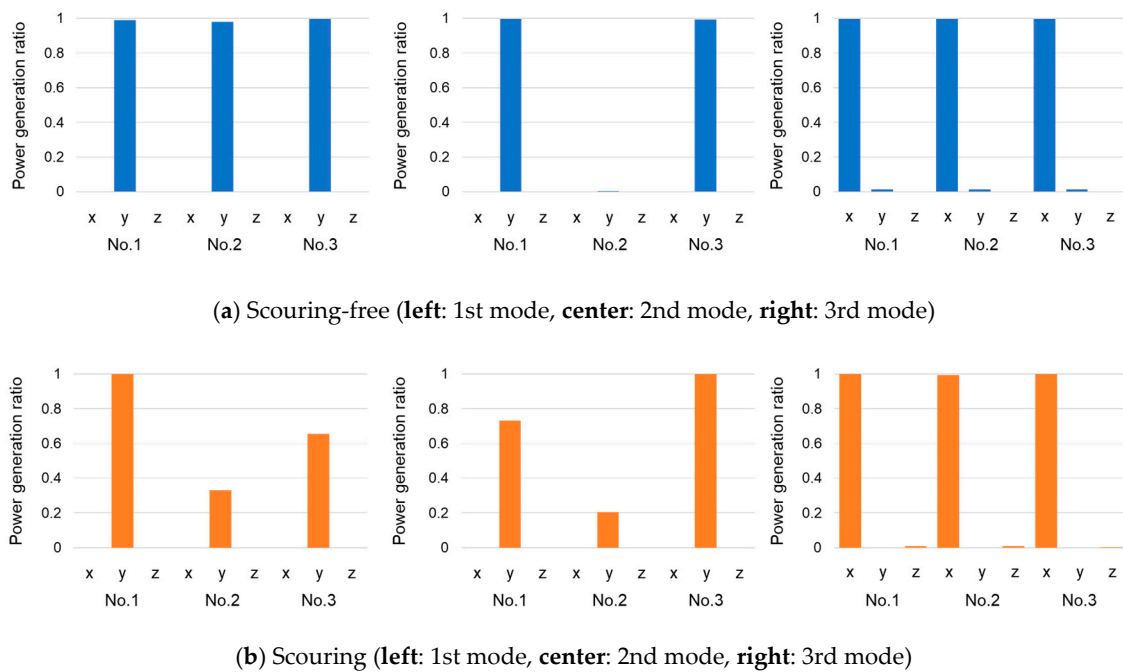


Figure 13. Output power generated by MEH (Pier model).

3.5. Detecting Pier Scour by Vibration-Based MEH

Figure 13 also implies that detecting the pier scour is possible if the power generated by the MEH devices are monitored in the x- and y-directions. Especially monitoring that at point No. 2, an obvious change in generated power could be observed when scour occurred.

Practically, as it is nearly impossible to obtain data from the perfectly scouring-free state, a scouring detection method that requires no reference state data (reference-free method) is of great importance. In Figure 13b, it is observed that when uneven scouring occurred, an unequal power was generated at the three observation points in the y-direction. Although the generated energy is small for the 3rd mode, this observation is also true as supported by a closer look in Figure 14 (subject to normalization with respect to the maximum out of the three observation points). When no uneven scouring occurred (the riverbed is flat), the power generated by the MEH at the three observations is almost equal.

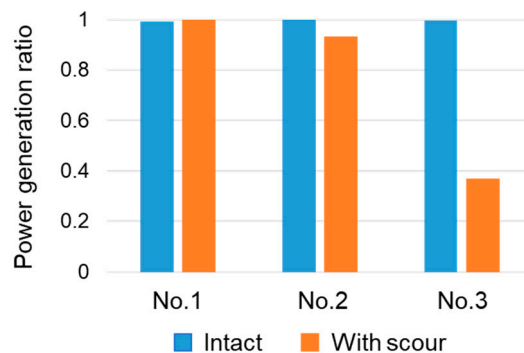


Figure 14. Power generation in the y-direction, 3rd mode.

Based on the observations above, a reference-free method could be proposed for detecting uneven pier scour using MEMS vibrational power generator devices as follows. (1) To install MEMS vibrational power generator devices at multiple observation points of equal height at the pier cap. The observation points are suggested to be one at the upstream side, one at the downstream side, and one in the middle; the selection of other observation points is not fully investigated yet and could be an open

question. (2) To monitor the power generated by the MEMS vibrational power generator devices in the longitudinal direction. If the powers generated at the observation points are unequal, it would be detected as uneven pier scour. In considering measurement noises, a certain threshold could be introduced to quantify the unequal powers, which is 5% in this study. The above proposal is limited to detecting uneven pier scours per the assumptions and modeling in this study. Further investigations could be conducted on detecting even pier scour and more complicated scouring states.

4. Conclusions

This study aimed to use a MEMS vibrational power generator to detect a bridge's slab damage and pier scour. Eigenvalue analysis of a bridge slab and pier using FEM models, in which slab damage was modelled by a reduced Young's modulus and pier scour was modelled by fixed boundaries of an inclined depth. In the eigenvalue analysis, the change in modal frequency and mode shape caused by the slab damage and pier scour consolidated the proposal of this present study.

Utilizing a electrostatic vibration-based MEMS–MEH, the change in natural frequency and amplitude could be monitored by the change in the generated power. A power generation index to detect the deteriorated panel in a slab was proposed and its applicability was verified with the numerical models. As for detecting uneven pier scour, a reference-free method was proposed with a MEMS vibrational power generator installed at multiple points of equal height at the cap and monitoring unequal generated powers. When an unequal power generation distribution is found, it may indicate the uneven pier scour.

The slab and pier models studied herein were simplified and the vibrations used to calculate the MEH generated energy were simply harmonic. The conclusions drawn above could apply only to the bridge types and damage patterns similar to those in this study. More complicated bridge types, models, and vibration patterns would help in generalizing the proposed methods.

Author Contributions: Conceptualization, K.H. and T.S.; formal analysis, K.H. and K.-C.C.; funding acquisition, T.S. and K.H.; investigation, K.H. and H.M.; methodology, K.H. and K.-C.C.; visualization, K.H. and H.M.; validation, K.H. and T.S.; supervision, T.S.; writing—original draft, K.H.; writing—review and editing, K.-C.C. and T.S. All authors have read and agreed to the published version of the manuscript.

Funding: This work was supported by JSPS KAKENHI Grant Number 20K04641.

Conflicts of Interest: The authors declare no conflict of interest.

References

1. Ministry of Land, Infrastructure, Transport and Tourism, Japan, Road Bureau. Roads in Japan. 2018. Available online: http://210.248.150.32/road/road_e/pdf/ROAD2018web.pdf (accessed on 14 October 2020).
2. Wang, H.; Hung, J.-J. Case study on foundation aberration of a river-crossing bridge in Taiwan. *Jpn. Geotech. Soc. Spéc. Publ.* **2016**, *2*, 1469–1473. [[CrossRef](#)]
3. Barbetta, S.; Camici, S.; Moramarco, T. A reappraisal of bridge piers scour vulnerability: A case study in the Upper Tiber River basin (central Italy). *J. Flood Risk Manag.* **2015**, *10*, 283–300. [[CrossRef](#)]
4. Zhang, J.; Peng, H.; Cai, C. Field Study of Overload Behavior of an Existing Reinforced Concrete Bridge under Simulated Vehicle Loads. *J. Bridg. Eng.* **2011**, *16*, 226–237. [[CrossRef](#)]
5. Fujiyama, C.; Maekawa, K. A Computational Simulation for the Damage Mechanism of Steel-Concrete Composite Slabs under High Cycle Fatigue Loads. *J. Adv. Concr. Technol.* **2011**, *9*, 193–204. [[CrossRef](#)]
6. Fathalla, E.; Tanaka, Y.; Maekawa, K. Effect of Crack Orientation on Fatigue Life of Reinforced Concrete Bridge Decks. *Appl. Sci.* **2019**, *9*, 1644. [[CrossRef](#)]
7. Toutlemonde, F.; Ranc, G. Fatigue tests of cracked reinforced concrete slabs for estimating the service life of composite bridge decks. *Rev. Française Génie Civ.* **2001**, *5*, 483–494. [[CrossRef](#)]
8. Chiew, Y.-M. Local Scour and Riprap Stability at Bridge Piers in a Degrading Channel. *J. Hydraul. Eng.* **2004**, *130*, 218–226. [[CrossRef](#)]
9. Xiong, W.; Cai, C.; Kong, B.; Zhang, X.; Tang, P. Bridge Scour Identification and Field Application Based on Ambient Vibration Measurements of Superstructures. *J. Mar. Sci. Eng.* **2019**, *7*, 121. [[CrossRef](#)]

10. Akbari, R.; Maadani, S.; Abedi, A.; Maalek, S. The effects of scour depth and riverbed condition on the natural frequencies of integral abutment bridges. *Struct. Monit. Maint.* **2019**, *6*, 85–101.
11. Boujia, N.; Schmidt, F.; Chevalier, C.; Siegert, D.; Van Bang, D.P. Effect of Scour on the Natural Frequency Responses of Bridge Piers: Development of a Scour Depth Sensor. *Infrastructures* **2019**, *4*, 21. [[CrossRef](#)]
12. Farahani, R.V.; Penumadu, D. Damage identification of a full-scale five-girder bridge using time-series analysis of vibration data. *Eng. Struct.* **2016**, *115*, 129–139. [[CrossRef](#)]
13. Fisher, M.; Atamturktur, S.; Khan, A. A novel vibration-based monitoring technique for bridge pier and abutment scour. *Struct. Health Monit.* **2013**, *12*, 114–125. [[CrossRef](#)]
14. Lin, Y.; Lai, J.-S.; Chang, K.; Chang, W.; Lee, F.; Tan, Y.-C. Using mems sensors in the bridge scour monitoring system. *J. Chin. Inst. Eng.* **2010**, *33*, 25–35. [[CrossRef](#)]
15. Keyaki, T.; Suzuki, O.; Uemura, S. 2B13 Development of a new scour detector that enables monitoring of pier soundness (Condition Monitoring-Vehicle). In Proceedings of the International Symposium on Seed-up and Service Technology for Railway and Maglev Systems: STECH, Chiba, Japan, 10–13 November 2015; Volume 2015, pp. 2B13-1–2B13-9.
16. Bryzek, J. Emergence of Trillion Sensors Movement. IEEE MEMS. 2014. Available online: https://site.ieee.org/scv-mems/files/2014/01/TSensors-1-22-14_final.pdf (accessed on 15 October 2020).
17. Kaminaga, M. Trillion Sensors and MEMS. *Sens. Mater.* **2018**, *30*, 723–731.
18. Roundy, S.; Wright, P.K.; Rabaey, J.M. *Energy Scavenging for Wireless Sensor Networks with Special Focus on Vibrations*; Springer: Norwell, MA, USA, 2004.
19. Saha, C.; O'Donnell, T.; Loder, H.; Beeby, S.; Tudor, J. Optimization of an Electromagnetic Energy Harvesting Device. *IEEE Trans. Magn.* **2006**, *42*, 3509–3511. [[CrossRef](#)]
20. Suzuki, Y. Recent progress in MEMS electret generator for energy harvesting. *IEEJ Trans. Electr. Electron. Eng.* **2011**, *6*, 101–111. [[CrossRef](#)]
21. Glynne-Jones, P.; Beeby, S.; White, N. Towards a piezoelectric vibration-powered microgenerator. *IEE Proc. Sci. Meas. Technol.* **2001**, *148*, 68. [[CrossRef](#)]
22. Koga, H.; Mitsuya, H.; Honma, H.; Fujita, H.; Toshiyoshi, H.; Hashiguchi, G. Development of a Cantilever-Type Electrostatic Energy Harvester and its Charging Characteristics on a Highway Viaduct. *Micromachines* **2017**, *8*, 293. [[CrossRef](#)] [[PubMed](#)]

Publisher's Note: MDPI stays neutral with regard to jurisdictional claims in published maps and institutional affiliations.



© 2020 by the authors. Licensee MDPI, Basel, Switzerland. This article is an open access article distributed under the terms and conditions of the Creative Commons Attribution (CC BY) license (<http://creativecommons.org/licenses/by/4.0/>).